Radiation Transport in Clouds

W. A. van Wijngaarden[1] and W. Happer[2]

[1]*Department of Physics and Astronomy, York University, Toronto, ON, Canada*

[2]*Department of Physics, Princeton University, USA*

Abstract

We briefly review the dominant role of clouds in Earth's climate. The earliest observational studies of heat transfer through Earth's atmosphere, for example, those of John Leslie around 1800, showed that clouds have a large effect on radiative heat transfer from Earth's surface to space. Greenhouse gases also affect heat transfer, but much less than clouds. For example, "instantaneously doubling" CO_2 concentrations, a 100% increase, only decreases radiation to space by about 1%. To increase solar heating of the Earth by a few percent, low cloud cover only needs to decrease by a few percent. The first half of this paper reviews observational facts about how clouds affect heat transfer. The second half gives a brief summary of the new 2n-stream radiation transfer theory for quantitatively analysing how clouds scatter radiation incident from outside the cloud, and how they emit thermal radiation generated by their particulates.

1. Role of Clouds in Earth's Climate

Some of the earliest quantitative work on radiative transfer and clouds was done by the Scottish physicist, John Leslie (1766-1832). He was the first to make quantitative measurements of downwelling radiation from the daytime and night time sky, that is, of the "sky temperature." He did this using a sensitive differential thermometer, which he called an "aethrioscope" shown in Fig. 1 [1].
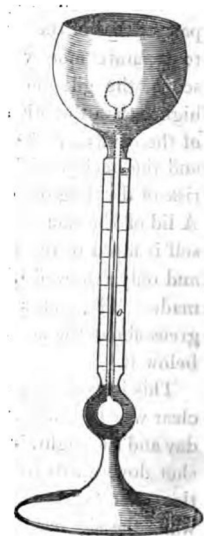

Figure 1:

An aethrioscope consists of two spherical glass bulbs, connected by a capillary tube containing a short column of alcohol (liquor) in the midsection. The lower bulb is shielded from radiation and held at room temperature. The upper bulb is at the focus of a parabolic reflector, a polished metal cup, which lets downward radiation focus on the bulb and heat it. Vice versa, thermal radiation emitted from the bulb is projected into the sky above. The cup plays much the same role as the dish antenna of a modern radar. The colder the apparent sky temperature, the higher the column of liquor is forced upward toward the absorbing-emitting bulb.

Leslie noticed substantial increases and decreases of downwelling radiation as clouds passed overhead, as described by his words: "*The sensibility of the instrument is very striking, for the liquor incessantly falls and rises in the stem with every passing cloud. In fine weather, the aethrioscope will seldom indicate a frigorific impression of less than 30 or more than 80 millesimal degrees (10 millesimal degrees = 1 C). If the sky become over clouded, may be reduced to as low as 15° or even 5° when the congregated vapours hover on the hilly tracts*" [2].

Even in 1800, Leslie was well aware that there were two kinds of radiation in the atmosphere, sunlight which you could see, and thermal radiation generated in the atmosphere, which we shall call earthglow, which one cannot see but can feel as radiant heat if it is sufficiently intense. Fig. 2 shows the spectral probability densities for short wave sunlight and for long wave earthglow. There is very little overlap between the two probability densities, which are equal at a wavelength of about λ= 4.2 μm. This can serve as a convenient boundary between "short wave" radiation or sunlight, and "long wave" thermal radiation or earthglow emitted by Earth's surface and atmosphere.
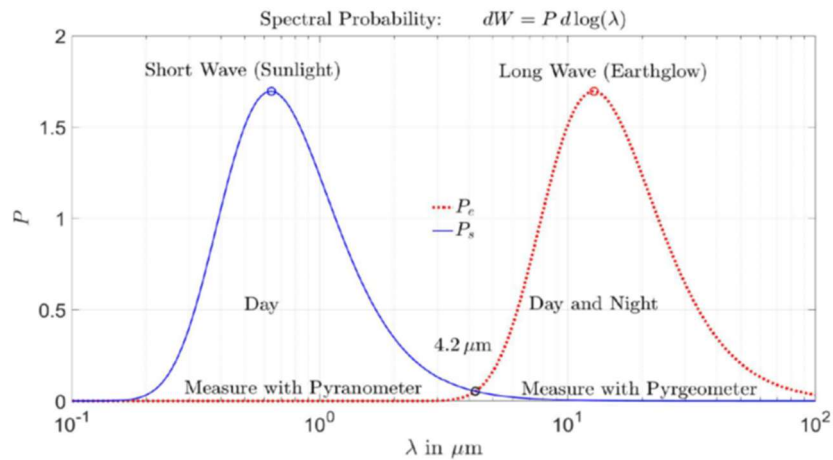

Figure 2: The spectral probability density for short wave sunlight, P_s, is shown as the blue curve and for long wave earthglow, P_e, as the red curve [3]. The increment $dW_i = P_i\, d\log\lambda$ is the infinitesimal probability to find the radiation energy of sunlight (i = s) or earthglow (i = e) with wavelengths corresponding to the interval between $\log\lambda$ and $\log\lambda + d\log\lambda$. The probability curves assume thermal radiation at a temperature of $T_s = 5772$ K for sunlight and $T_e = 288.7$ K for earthglow.

The two types of radiation can be measured with two types of instruments, a *pyranometer* for detecting sunlight and a *pyrgeometer* to measure earthglow. Leslie's aetherioscope was sensitive to both direct and scattered sunlight as well as to thermal radiation emitted by clouds and greenhouse gases. It detected radiation from a relatively narrow range of directions near the vertical. One modern instrument that has evolved from the aetherioscope is the *pyranometer,* an example of which is illustrated in Fig. 3.
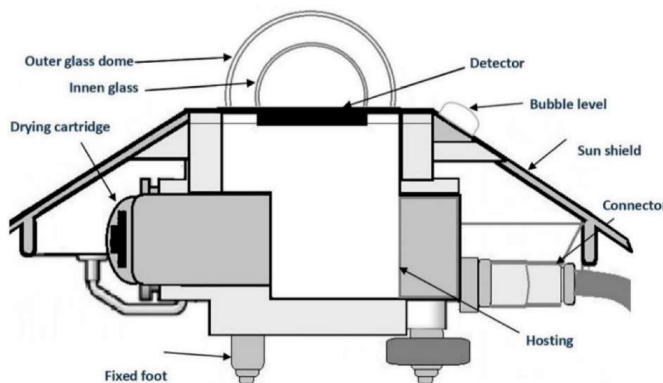

Figure 3: A pyranometer consists of a detector that absorbs solar radiation that is sealed by two glass domes to protect the sensor from the elements [4]. The instrument's sensitivity depends on the wavelength response of the detector. Silicon-based diodes typically detect wavelengths in the range of 0.3 – 1.2 μm where most solar panels operate.
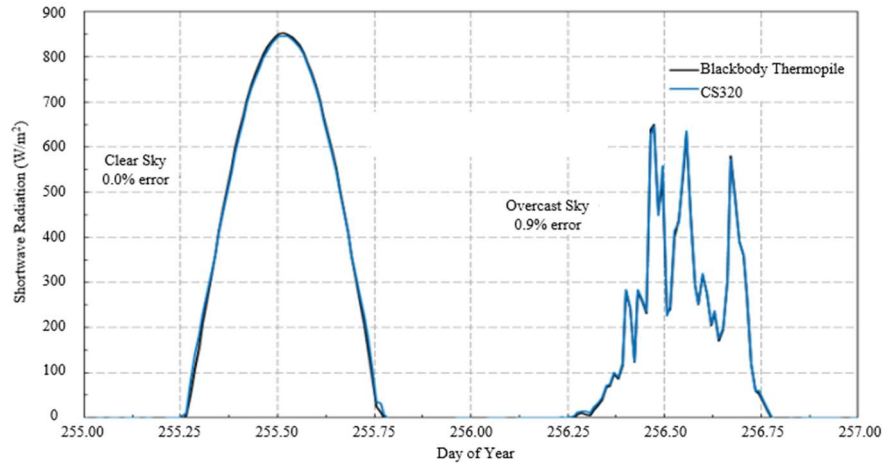
Figure 4: Pyranometer Measurements of Solar Flux at Earth's Surface at Utah, USA in August. This data was obtained using a Campbell Scientific CS320 model pyranometer [5] and compared to that obtained using a thermopile.

Fig. 4 was generated by Campbell Scientific, a pyranometer manufacturer. It shows that for measuring solar radiation, an instrument built with a sensitive photoelectric detector, CS320, yields results that are nearly identical to that using a much less sensitive thermopile. The results show a dramatic difference in shortwave radiation reaching the Earth's surface for a clear sky as compared to an overcast day. But Mother Nature is subtle. Paradoxically, Fig. 5 shows skies with lots of clouds can increase the solar flux on some ground patches while decreasing it on others. The highly reflecting water droplets of the cloud edges forward-scatter sunlight and add to the direct irradiance from the sun.
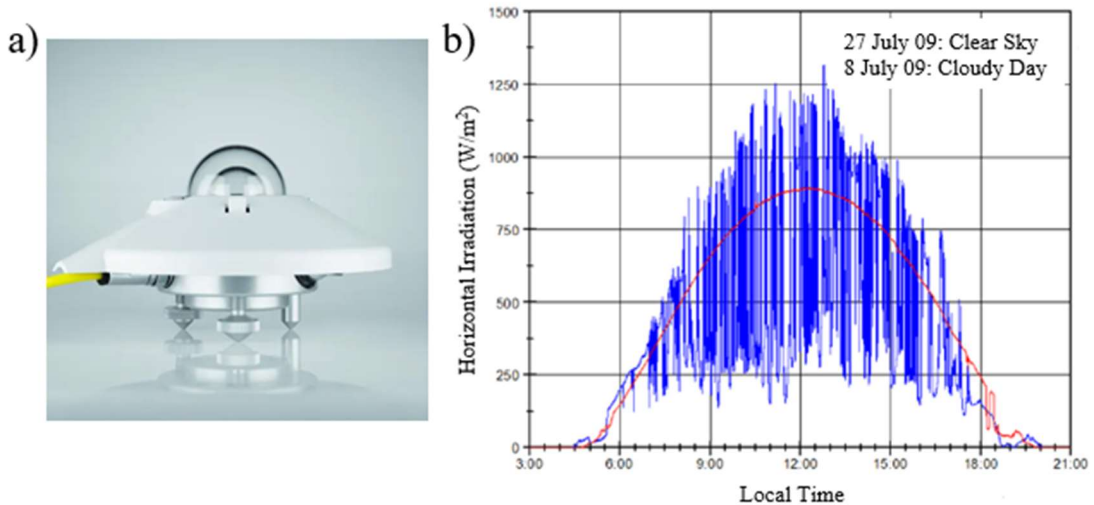

Figure 5: A Kipp & Zonen CMP22 Pyranometer [6] was used to show how clouds affect the solar irradiance measured at Munich Germany on July 8, 2009 when it was cloudy (blue) and July 27, 2009 when the sky was clear (red) [7].

An instrument that complements the pyranometer is the pyrgeometer illustrated in Fig. 6, which is designed to see only the downwelling flux from thermal emission by greenhouse gases and clouds in the atmosphere. A silicon dome and thin-film spectral filters prevent all solar radiation from reaching the detector, which is "solar blind." But the dome and filters admit most radiation with wavelengths between 4.2 to 50 μm, which includes nearly all atmospheric thermal radiation or earthglow. Upward thermal radiation emitted from the detector surface can pass back through the filters and dome into the cold sky. The upward-facing detector surface will normally be colder

than the bottom since the sky is usually colder than the pyrgeometer. A modern pyrgeometer is designed to do just what John Leslie's aethrioscope did, to measure how cold the sky is.
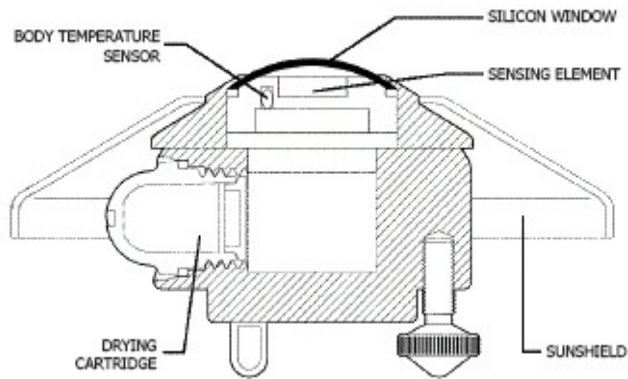

Figure 6: An instrument that complements the pyranometer is the pyrgeometer [8], which is designed to see only the downwelling flux from thermal emission by greenhouse gases and clouds in the atmosphere. A silicon dome and thin-film spectral filters prevent all solar radiation from reaching the detector, which is "solar blind." However, the dome and filters admit most radiation with wavelengths between 4.2 to 50 µm, which includes nearly all atmospheric thermal radiation or earthglow.

Fig. 7 shows a two-week recording of downwelling thermal radiation measured with a pyrgeometer at Thule, Greenland in July. There is very little variation of downwelling radiation from day to night. But there is a large difference between clear and cloudy weather, with close to 340 W/m^2 downwelling from cloud bottoms on overcast days and around 260 W/m^2 in clear weather, where the downwelling comes primarily from thermal emission of water vapor, H_2O, and carbon dioxide, CO_2. The cloud bottoms produce the same flux as a blackbody with a temperature of about 5 C. The clear sky produces the same flux as a blackbody at a temperature of about -13 C. Figures 5 and 7 show downwelling radiation onto Earth's surface. But upwelling radiation to space is qualitatively similar.
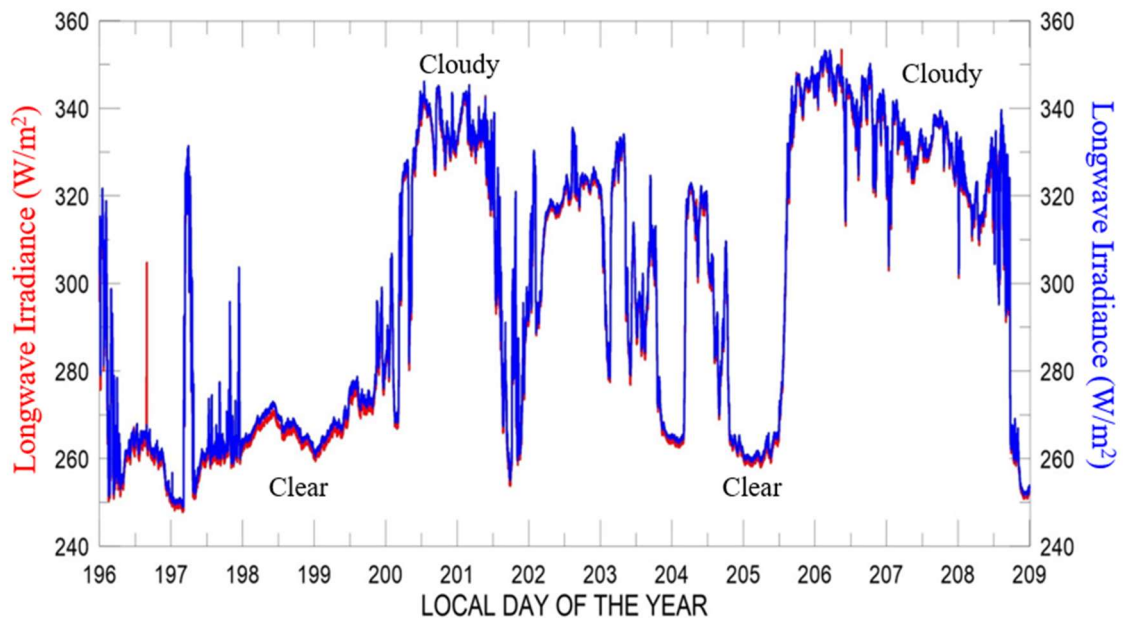

Figure 7: Comparison of downward longwave irradiance measured at the The Thule High Arctic Atmospheric Observatory (THAAO), Greenland in 2016 using two Kipp & Zonen Model CGR4 pyrgeometers calibrated in 2012 (red) and 2014 (blue) [9]. Note the suppressed zero on the vertical scale! The downwelling from cloudy skies is only about 30% greater than that from clear skies.

Fig. 8 shows longwave infrared and visible images of the Earth, recorded at the same time by a geosynchronous satellite parked in the equatorial plane above Ecuador. The right side of Fig. 8 shows blue sunlight at a wavelength of 0.47 μm diffusely reflected in the late afternoon retrieved at 6:12 pm in Princeton, New Jersey. Night has already descended on Europe and the eastern Atlantic so the right side of the image appears dark. The left side of Fig. 8 shows that Earth "glows in the dark," at a wavelength of 10.3 μm, in the "infrared window," where there is little absorption by greenhouse gases in cloud-free skies. So much heat is stored up from the previous day that the nighttime side of the globe on the right is just as bright with longwave radiation as the daytime side on the left. Like the pyrgeometer measurements of downward earthglow in the previous viewgraph, the earthglow seen from space has nearly the same intensity day or night.
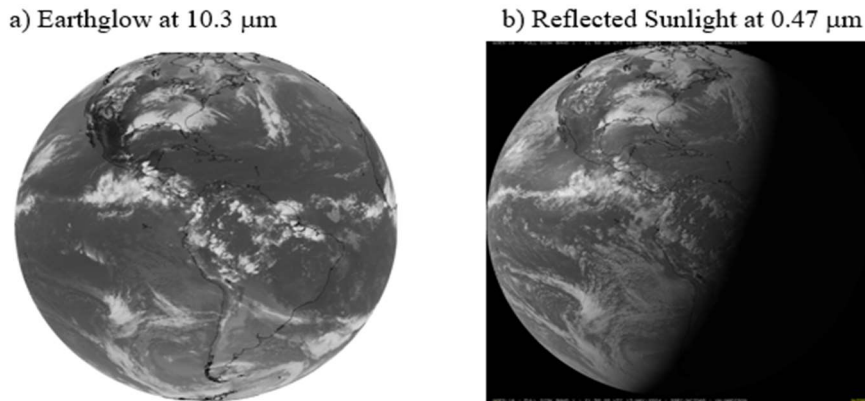

Figure 8: Satellite images retrieved at 6:12 pm EST on May 13, 2024 [10] of a) Earth-glow measured at 10.3 μm and b) reflected sunlight measured at 0.47 μm.

The right column of Fig. 9 shows spectra of long wave thermal infrared radiation that reaches the satellite from a cloud-free area of the Earth. On the left are theoretically modelled spectra. One can hardly tell the difference between the modelled and observed spectra.
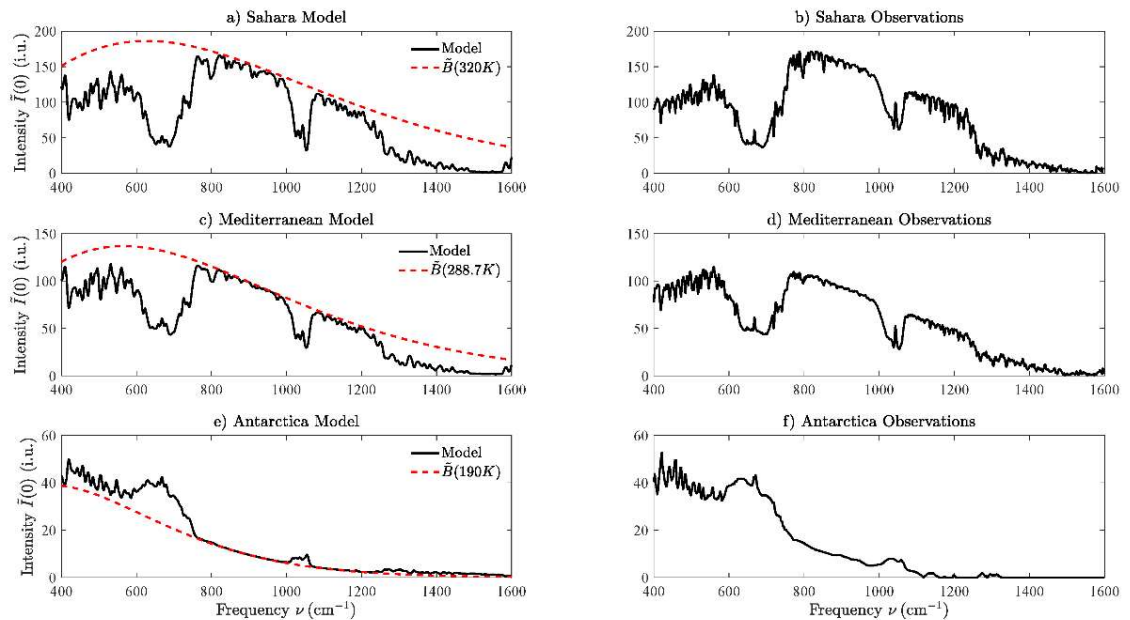
Figure 9: Comparison of modeled for a clear sky with data observed by a Michaelson interferometer in a satellite over the Saharan desert, the Mediterranean and Antarctica [11]. The intensity unit is 1 i.u. = 1 mW m^{-2} cm sr^{-1}. Radiative forcing is negative over wintertime Antarctica since the relatively warm greenhouse gases in the troposphere, mostly CO_2, O_3 and H_2O radiate more to space than the cold ice surface at a temperature of T = 190 K, could radiate through a transparent atmosphere.

The top of the atmosphere fluxes come from solutions of the Schwarzschild equation [12]

$$\mu \frac{\partial}{\partial z} I(z, \mu) = \alpha(z)[B(z) - I(z, \mu)]$$

for the intensity $I(z, \mu)$ with direction cosine $\mu = \cos \theta$, at the altitude z, where α is the attenuation absorption coefficient and the Planck intensity is $B(z)$ [13]. $\theta = 0$ corresponds to upwards intensity while $\theta = \pi$ corresponds to downward intensity. Fig. 10 shows the frequency dependence of the spectral flux at the top of the atmosphere for the case of a cloudless sky for various concentrations of carbon dioxide.
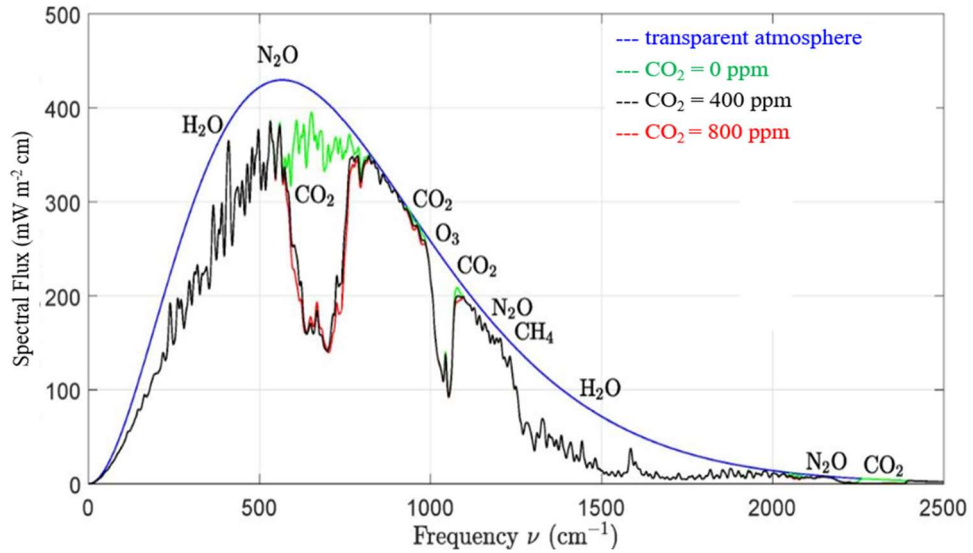

Figure 10: Effect of changing concentrations of carbon dioxide CO_2, on the spectral flux at the top of the atmosphere [11]. *The smooth blue line is the spectral flux from a surface at the temperature of 288.7 K for a transparent atmosphere with no greenhouse gases. The green line is with all CO_2 removed but with all the other greenhouse gases at their standard concentrations. Similarly, the black and red lines were found for CO_2 concentrations of 400 and 800 ppm, respectively. Doubling the concentration of CO_2 from 400 to 800 ppm would cause a forcing increase (the area between the black and red lines) of 3.0 W/m^2.*

2. 2n-Stream Radiation Transfer Theory

To model radiation inside and outside of clouds, one must also take scattering of radiation into account. This is described by the equation of transfer [14]

$$\frac{1}{\alpha(\mathbf{r})} (\mathbf{n} \cdot \nabla) I(\mathbf{r}, \mathbf{n}) - \frac{\widetilde{\omega}(\mathbf{r})}{4\pi} \int_{4\pi} d\Omega' \ p(\mathbf{r}, \mathbf{n}, \mathbf{n}') I(\mathbf{r}, \mathbf{n}') = [1 - \widetilde{\omega}(\mathbf{r})] B(\mathbf{r})$$

Here, the independent variables are

$\mathbf{r}$ = spatial location in atmosphere; $\nabla = \partial/\partial \mathbf{r}$

$\mathbf{n}$ = directional unit vector, centered in solid-angle increment $d\Omega = \sin \theta d\theta d\phi$

The "knowns" at the spatial location r are

$\alpha(\mathbf{r})$ = attenuation coefficient from scattering and absorption

$\widetilde{\omega}(\mathbf{r})$ = single scattering albedo (fraction scattered instead of absorbed)

$B(\mathbf{r})$ = Planck intensity; depends on local temperature $T(\mathbf{r})$

$p(\mathbf{r}, \mathbf{n}, \mathbf{n}')$ = phase function; $p(\mathbf{r}, \mathbf{n}, \mathbf{n}')d\Omega'/4\pi$ is probability to scatter radiation from initial direction $\mathbf{n}'$ into solid-angle increment $d\Omega$ centered on final direction $\mathbf{n}$

The unknown is

$I = I(\mathbf{r}, \mathbf{n}) =$ Intensity or radiance along unit vector $\mathbf{n}$ at spatial location $\mathbf{r}$.

The solution of this integro differential equation is discussed in our papers on 2n-Stream Radiative Transfer [15] and Radiative Transfer in Cloud Layers [16]. Despite the vast funds poured into climate research, the properties of clouds needed to solve the equation of transfer can only be described as "knowns" in quotation marks. Single scattering albedos, $\tilde{\omega}$, phase functions, p, attenuation coefficients, α, and other properties of cloud particulates are not very well known from experimental observations.

Monte Carlo simulations can give qualitative insight into solutions of the equation of transfer for just about any complicated state of a cloudy atmosphere [17]. For a more systematic, quantitative understanding one can find analytic solutions for simplified limiting situations, which preserve most of the important physics of the problem. We apply a technique we call the 2n-Stream Radiative Transfer that solves the radiative transfer equation for a 1-dimensional column of atmosphere [15, 18, 19].

The basic idea of 2n-stream radiative transfer theory was developed in 1943 by Gian Carlo Wick [20] to analyze neutron transport by multiple scattering. Wick's two key steps were to first consider only axially symmetric radiation transfer, i.e., the intensity $I(\mathbf{r}, \mathbf{n}) \to I(z, \mu)$ and next evaluate the scattering integral with a sum on $2n$ sample values μ_i of the direction cosines μ, a so-called Gaussian quadrature [21].

$$\int_{4\pi} d\Omega' p(\mathbf{n}, \mathbf{n}') I(\mathbf{n}') \to 2\pi \int_{-1}^{1} d\mu' p(\mu, \mu') I(\mu') \to 2\pi \sum_{i'=1}^{2n} p(\mu_i, \mu_{i'}) w_i I(\mu_{i'})$$

Wick's sampling is closely analogous to Shannon-Nyquist sampling of communications signals [22]. But unlike the equally-weighted Shannon-Nyquist sample times, each of the $2n$ Gauss-Legendre sample direction cosines μ_i has a different weight w_i given in terms of the Legendre polynomials P_l by

$$\frac{1}{w_i} = \sum_{l=0}^{2n-1} \frac{2l+1}{2} P_l^2(\mu_i)$$

Scattering and emission can then be represented by 2n x 2n matrices which describe how 2n incident beams are scattered into 2n output beams. For 2n-stream radiation transfer calculations, the axially symmetric phase function, $p(\mathbf{n}, \mathbf{n}')$, is replaced by a 2n x 2n matrix of sample values $p(\mu_i, \mu_{i'})$, evaluated at the Gauss-Legendre direction cosines, μ_i and $\mu_{i'}$. Some examples are shown in Fig. 11.
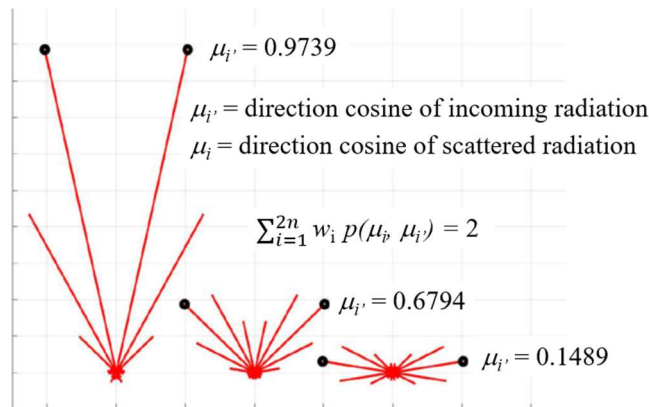

Figure 11: Forward Scattering Phase Function $p(\mu_i, \mu_{i'})$ for Cloud Particulates [1].

For simplicity, we assume only 2n = 10 streams of axially symmetric radiation. Scattering for three different input directions are shown, highly vertical on the left, highly horizontal on the right and intermediate in between. This example is the maximum forward-scattering phase function, that is nonnegative for any input or output direction cosines, and that can be constructed from the first six Legendre polynomials, P_0, P_1, ..., P_5. Acceptable phase functions are rotationally symmetric, nonnegative and satisfy the sum rule shown in Fig. 11.

When solving the equation of transfer, it is convenient to make a distinction between radiation that is generated by thermal emission of molecules and particulates inside the cloud, which we denote by $\dot{I}$ and radiation in the cloud that has come from external sources like sunlight, or thermal emission of Earth's surface, which we denote by $\ddot{I}$. Fig. 12 illustrates the difference between $\dot{I}$ and $\ddot{I}$.
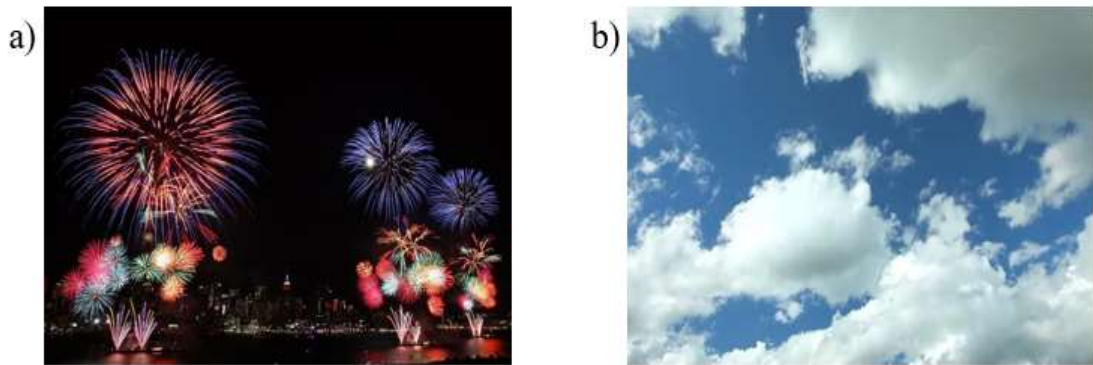

Figure 12: The left figure (a) shows thermal emission, i.e. visible light emitted by very hot atoms or particulates, in this example by fireworks, but also by lightning, aurora etc. Long wave infrared radiation is emitted by greenhouse gas molecules and particulates at normal atmospheric temperatures. The right figure (b) shows scattered white sunlight from particulates of water or ice (clouds), and blue, Rayleigh-scattered sunlight from N_2 and O_2 in cloud-free air. Scattered long wave infrared radiation comes only from particulates, for example, the water or ice particulates of clouds. There is negligible scattering of long wave radiation by molecules.

Fig. 13 shows a calculation done with 2n scattering theory. In this example 2n = 10. An isothermal cloud layer is located between the green lines at optical depths 0 and 8 above the bottom. Incident radiation is generated by a black body located below the cloud.

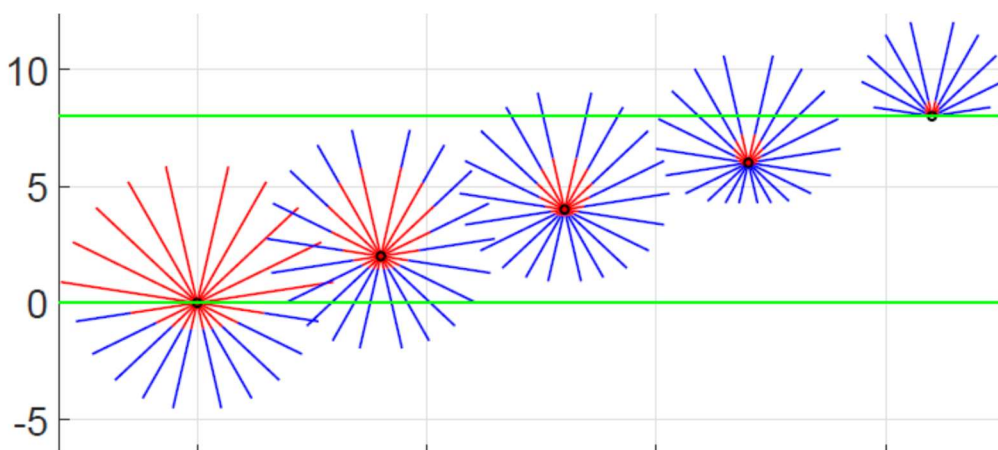*Figure 13: Scattering in an isothermal cloud. The green lines show the bottom and top of a cloud layer at optical depths $\tau = 0$ and $\tau = 8$. The blue rays show intensities thermally generated by isothermal cloud particulates with a Planck Intensity B. The red rays show incident and scattered intensities from a black body located below the cloud. The black body is warmer than the cloud and has a 20% larger Planck intensity.*

For studies of climate, the behavior of radiation inside a cloud is of little importance compared to the properties of radiation escaping from the cloud top to space or from the cloud bottom to irradiate Earth's surface. The external incoming intensity $\ddot{I}^{\{in\}}$, consisting of n upward external streams incident on the bottom of the cloud and n downward external streams, incident on the top of the cloud generates an outgoing intensity $\ddot{I}^{\{out\}}$ consisting of n upward scattered streams emerging from the top of the cloud, and n downward scattered streams emerging from the bottom of the cloud. The constant of proportionality between the weighted 2n incoming streams $\ddot{I}^{\{in\}}$ and 2n outgoing streams $\ddot{I}^{\{out\}}$ is the 2n x 2n scattering matrix S. For real clouds, some fraction of the incoming radiation is always absorbed and heats the scattering particulates.

For thermal radiation intensity, $\dot{I}^{\{out\}}$, emerging from an isothermal cloud, the n upward streams emerging from the top and the n downward streams emerging from the bottom are proportional to the 2n streams of the isotropic Planck intensity B in the cloud. The constant of proportionality is the emissivity matrix $\mathcal{E}$.

Fig. 14 shows on the lower left side the incoming radiation (red) into the bottom of the cloud shown in Fig. 13. On the lower right of Fig. 14 is the outgoing scattered radiation out of the top and bottom of the cloud layer shown in Fig. 13. Thermal radiation (blue) generated in the cloud is emitted isotropically as illustrated in the top left of Fig. 14. The upper right diagram shows the thermal radiation that escapes from the top and bottom of the cloud. Note the thermal radiation rays that are emitted closest to the horizontal direction travel a greater distance in the cloud and therefore experience greater absorption than the rays directed upward/downward.

In an interesting generalization of Kirchhoff's law [23] to 2n-stream scattering theory, the sum of the scattering matrix S and the emissivity matrix $\mathcal{E}$ is the identity matrix 1, that is $S + \mathcal{E} = 1$. The effects of the scattering matrix S and emissivity matrix $\mathcal{E}$ used in Fig. 13 are shown in Fig. 14.

$$w_i\, \dot{I}^{\{out\}}(\mu_i) = \sum_{i'} \mathcal{E}_{ii'}\, w_{i'}\, B(\mu_{i'})$$

$\mathcal{E}$ = Emissivity Matrix

$$w_i\, \ddot{I}^{\{out\}}(\mu_i) = \sum_{i'} S_{ii'}\, w_{i'}\, \ddot{I}^{\{in\}}(\mu_{i'})$$
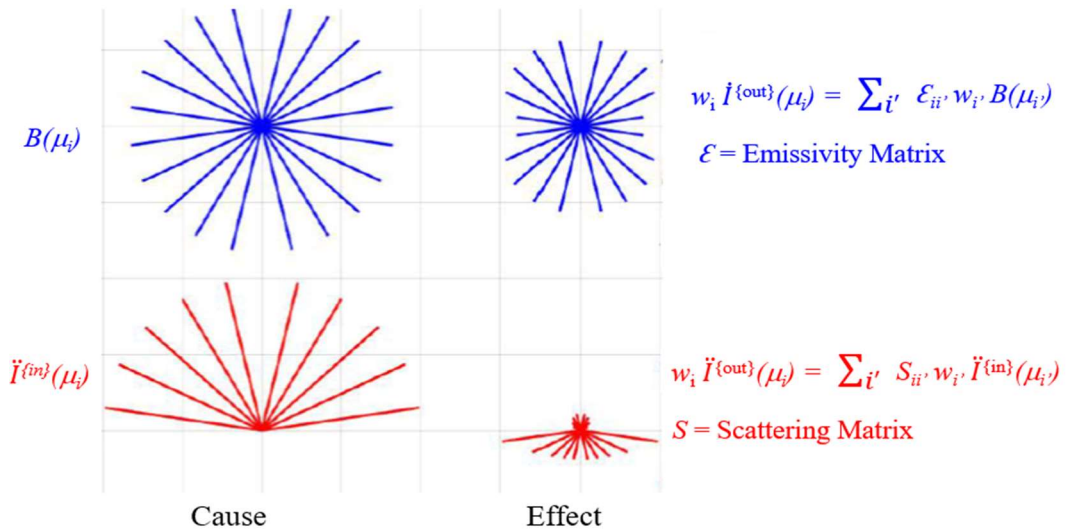
S = Scattering Matrix

Cause   Effect

Figure 14: The left side shows the incoming radiation (red) into the bottom of the cloud shown in Fig. 13 as well as thermal radiation (blue) that is generated isotropically inside the cloud. The right side shows the effect of scattering and absorption. The scattering S and emissivity $\mathcal{E}$ matrices sum to unity in accordance with Kirchhoff's law.

3. Conclusion

In conclusion, radiative transfer theory shows that doubling the concentration of the most important anthropogenic greenhouse gas, carbon dioxide, for a cloudless sky only decreases radiation to space by 1%. However, clouds cover more than half the planet [24] as shown by the iconic Blue Marble photograph [25] in Fig. 15. An increase in low cloud cover of only about 1% could largely compensate for the doubling of CO_2 [26].

Figure 15: The Blue Marble [24]. *A photograph of Earth and its clouds by lunar astronaut Harrison Schmitt taken on December 7, 1972.*

2n-stream radiative transfer theory is an invaluable tool to model clouds and particulates such as aerosols that scatter infrared radiation. It is essential that accurate measurements of cloud parameters such as the single scattering albedo, optical depth and scattering phase function be made as these quantities are essential inputs into any calculation. The dependence of these parameters on infrared wavelength as well as an understanding of how they vary for clouds at different altitudes or consisting of different amounts of water droplets and ice crystals is essential for meaningful progress in climate modelling.

Editor: Hermann Harde

References

1. John Leslie, https://en.wikipedia.org/wiki/John_Leslie_(physicist), accessed Dec. 11, 2024.

2. J. Leslie, *A short account of experiments and instruments, depending on the relations of air, to heat, and moisture,* (1813). https://archive.org/details/shortaccountofex00lesliala.

3. M. T. Rose, A. N. Crossan & I. R. Kennedy, *Sustaining Action and Optimizing Entropy: Coupling Efficiency for Energy and the Sustainability of Global Ecosystems*, Bulletin of Science Technology & Society, **28**, No. 3, 260-272 (2006).

4. R. Mubarak, H. Schilke & G. Seckmeyer, *Improving the Irradiance Data Measured by Silicon-Based Sensors*, Energies, **14**, 2766 (2021). https://doi.org/10.3390/ en14102766.

5. C. Stephens, *Measuring the Sun More Accurately and Simply*, Campbell Scientific (2017). https://www.campbellsci.ca/blog/measuring-sun-accurately-simply

6. Kipp & Zonen CMP22 Pyranometer, https://www.otthydromet.com/en/p-kippzonen-cmp22-pyranometer/0362930, accessed Dec. 12, 2024.

7. M. Zehner et al, *Systematic Analysis of Meteorological Irradiation Effects* (2010). www.researchgate.net/publication/237353475_Systematic_Analysis_of_Meteorological_Irradiation_Effects

8. Pyrgeometer, https://en.wikipedia.org/wiki/Pyrgeometer, accessed Dec. 12, 2024.

9. D. Meloni, *Shortwave and longwave broadband radiometers*, The Thule High Arctic Atmospheric Observatory (THAAO), Greenland, https://www.thuleatmos-it.it/instruments/radiometers/index.php, accessed Dec. 12, 2024.

10. SSEC Geostationary Satellite Imagery, https://www.ssec.wisc.edu/data/geo/#/animation

11. W. A. van Wijngaarden & W. Happer, *Dependence of Earth's Thermal Radiation on Five Most Abundant Greenhouse Gases*, Atmospheric and Oceanic Physics*, (2020) arXiv: 2006.03098.

12. K. Schwarzschild, *Űber Diffusion und Absorption in der Sonnenatmosphäre,* Nachr. K. Gesell. Wiss. Math.-Phys. Klasse, **195**, 41 (1906).

13. M. Planck, *The Theory of Heat Radiation*, (1914), translated by M. Masius, (2nd ed.). P. Blakiston's Son & Co.

14. S. Chandrasekhar, *Radiative Transfer*, Dover, New York (1960).

15. W. A. van Wijngaarden & W. Happer, *2n-Stream Radiative Transfer*, Atmospheric and Oceanic Physics (2022) arXiv: 2205.09713.

16. W. A. van Wijngaarden & W. Happer, *Radiation Transfer in Cloud Layers*, Atmospheric and Oceanic Physics (2023) arXiv: 2310.10622.

17. J. Steinacker, M. Baes & K. D. Gordon, *Three-Dimensional Dust Radiative Transfer*, Annual Rev. Astron. Astrophys. 51, 63-104 (2013) doi: 10.1146/annurev-astro-082812-141042.

18. G. E. Thomas & K. Stamnes, *Radiation Transfer in the Atmosphere and Ocean*, Cambridge University Press, Cambridge, England (1999).

19. P. Eriksson, S. A. Buehler, C. P. Davis, C. Emde & O. Lemke, *ARTS, the atmospheric radiative transfer simulator, Version 2*, J. Quant. Spect. Rad. Trans. **112** (10): 1551–1558 (2011).

20. G. C. Wick, *Űber ebene Diffusionsprobleme*, Z. Phys. **121**, 702 (1943).

21. Gauss-Legendre quadrature, https://en.wikipedia.org/wiki/Gauss%E2%80%93Legendre_quadrature

22. C. E. Shannon, *Communication in the presence of noise*, Proceedings of the Institute of Radio Engineers, **37** (1): 10-21 (1949). https://en.wikipedia.org/wiki/Nyquist%E2%80%93Shannon_sampling_theorem

23. Kirchhoff's laws of thermal radiation, https://en.wikipedia.org/wiki/Kirchhoff%27s_law_of_thermal_radiation

24. CERES: *Clouds and the Earth's Radiant Energy System*, https://ceres.larc.nasa.gov, accessed 24 Oct. 2023.

25. https://en.wikipedia.org/wiki/The_Blue_Marble

26. NASA Earth Observatory, *Clouds & Radiation*, https://earthobservatory.nasa.gov/features/Clouds#:~:text=Low%2C%20thick%20clouds%20primarily%20reflect,the%20surface%20of%20the%20Earth , accessed Dec. 16, 2024.